AIAA JOURNAL
Vol. 40, No. 1, January 2002

Relaxation of Turbulent Boundary Layer Submitted to Sudden Distortion at the Wall

N. Nait Bouda* and T. Benabid†
University of Sciences and Technology Houari Boumediène, C.P 16111 Algiers, Algeria
and
L. Fulachier‡
Institut de Recherches sur les Phénomenes Hors Equilibre, 13003 Marseille, France

An experimental investigation is carried out in the turbulent boundary layer subjected to a sudden transverse strain, which generates strong three-dimensional effects. Particular attention is focused on the reorganization of the distorted boundary layer into a two-dimensional one on a stationary cylinder downstream an axially rotating part. The physical behavior of the flow is analyzed through the mean and turbulent velocity field. The results show three zones: an interaction zone where the flow responds to the new boundary condition (cessation of spin), an adjacent one where the influence of the rotation remains persistent on the flow structure, and an outer undisturbed zone where the flow remains in equilibrium.

Nomenclature

a	=	radius of cylinder
$E(n)$	=	spectral density of velocity fluctuations
P	=	local static pressure
P_e	=	freestream static pressure
q	=	local velocity ($q = \bar{q} + q'$)
q'	=	velocity fluctuations
$\bar{q}$	=	mean velocity (rotation case)
q_e	=	mean outer velocity
R	=	turbulence Reynolds number
$R_{u'w'}$	=	relative correlation coefficient to u' and w'
R_θ	=	Reynolds number based on momentum thickness
S	=	absolute coordinate system
$\underset{\sim}{S}$	=	relative coordinate system
T	=	integral timescale
U_e	=	freestream velocity
u'	=	longitudinal velocity fluctuations in S
$\underset{\sim}{u}'$	=	longitudinal velocity fluctuations in $\underset{\sim}{S}$
$\bar{u}$	=	longitudinal mean velocity component in absolute coordinate system
$\underset{\sim}{\bar{u}}$	=	longitudinal mean velocity component in relative coordinate system
W_0	=	peripheral velocity
w'	=	transverse velocity fluctuations in S
$\underset{\sim}{w}'$	=	transverse velocity fluctuations in $\underset{\sim}{S}$
$\bar{w}$	=	transverse mean velocity component in absolute coordinate system
$\underset{\sim}{\bar{w}}$	=	transverse mean velocity component in relative coordinate system
x	=	axial length measured from the leading edge of the spinning part
x_f	=	axial length measured from the leading edge of the fixed part
β	=	streamlines deviation
δ	=	boundary-layer thickness
δ_0	=	boundary-layer thickness at $x = -25$ mm
ε	=	viscous dissipation rate
Λ	=	integral length scale of velocity fluctuations
λ	=	dissipation scale
ν	=	kinematic viscosity
π	=	Clauser parameter
ρ	=	density of the fluid
τ	=	times decay

Received 1 November 1999; revision received 18 May 2000; accepted for publication 16 March 2001.

*Research Scientist, Laboratoire de Mécanique des Fluides, B.P. 32 Bab Ezzouar.
†Lecturer, Laboratoire de Mécanique des Fluides, B.P. 32 Bab Ezzouar.
‡Director of Research, 12, Avenue du General Leclerc.

I. Introduction

STUDY of three-dimensional turbulent flows presents a particular interest in getting up some properties of turbulence that are frequently masked in two-dimensional configuration. Therefore, three-dimensional flows constitute a test for theories that work very well in most cases of two-dimensional flows. Frequently, turbulence models developed for two-dimensional turbulent boundary layers are extended to three-dimensional turbulent boundary layers. However, they give poor results owing to significant changes in turbulence structure. So, several reviews including those of Launder[1] and Purtell[2] continued to recognize the need for more detailed turbulent measurements to get advanced methods for modeling turbulence in three-dimensional turbulent boundary layers.

In practice, three-dimensional flows usually arise from transverse pressure gradients, such as those that occur on swept wings, rotating turbines, or on curved ducts. Likewise, most experiments used transverse pressure gradients to generate a crossflow.[3–7] The inconvenience of this type of geometry is that the flow is strongly influenced by pressure gradients, which certainly can conceal important aspects of the interaction between turbulent stresses and mean velocity field. We note, however, that many three-dimensional boundary layers are caused by a transverse shear. An innovative experiment was devised by Furuya and Nakamura.[8] They studied the growth of crossflow produced by a spinning cylinder aligned with a uniform flow, but they did not report turbulence measurements. Bissonette and Mellor[9] and Lohmann[10] later reported turbulence results on a similar experiment, but they have not explored the region very close to the wall, which plays a crucial role.

A further experimental and computational analogous study was performed at the Institut de Mecanique Statistique de Turbulence (Institut de Recherches sur les Phénomenes Hors Equilibre, Marseille).[11–20] The experiment is carried out in the boundary layer on an axially rotating cylinder following a stationary one so that the fully developed upstream two-dimensional turbulent boundary layer is suddenly submitted to a transverse strain. This generates complex three-dimensional effects, which are studied through their influence on the mean and turbulent velocity fields. The authors[13,14,20] showed that the experimental results obtained in an absolute coordinate

system within the rotation layer lead to misinterpretation. These results must be examined in a relative system far downstream the leading edge of the spinning part. It appears also that many difficulties arise in the turbulence modeling, particularly in the region very close to the wall. The anisotropic viscosity k-ε model performed by Cousteix et al.[19] does not agree with experimental results.

Another feature of study in rapidly changing mean rate of strain at the wall is the experimental observation of the turbulence response to a cessation of spin. It should serve as a useful guideline for complementary hypothesis for any theory.

To our knowledge, only one experiment has been performed in this way to date. It concerns the work of Driver and Hebbar.[21] The authors presented flowfield measurement as a continuation of Higuchi and Rubesin's[22] work. A three-component laser Doppler velocimeter was used to measure three components of mean velocity and six Reynolds stresses. The authors have compared the data with several turbulence models. They deduced that calculation using a Reynolds stress equation turbulence model generally agreed well with the data. Although, some meaningful results had been obtained; no systematic comparison had been done with the no-spinning case. The objective of the experience carried at the University of Sciences and Technology Houari Boumediène (USTHB) is to get complementary flowfield measurement in the relaxing three-dimensional boundary layer on the fixed part of a cylinder downstream of the rotating section.

Otherwise, we note some ambiguity in the manner to approach the flow. Indeed, one can no longer observe the flow from a relative coordinate system. On the other hand, an absolute system is not entirely suitable, especially to the vicinity of the spinning cylinder where it produces a rotation of the flow. Such a situation sets a fundamental problem, which remains unresolved at the moment.

II. Flowfield Geometry and Instrumentation

The experiments were conducted in the open wind (600 × 1000 mm) (USTHB, Algiers). The experimental model is that used at the Institut de Recherches sur les Phénomenes Hors Equilibre (IRPHE)[20]; it deals with a metallic circular cylinder of diameter $2a = 197$ mm. The stationary downstream part, which followed the rotating cylinder, is extended in order to observe the relaxation of the boundary layer on this part.

The scheme (Fig. 1) shows the geometrical configuration.

To create a transverse friction of the same order as the longitudinal one, the wall velocity has been chosen close to the freestream velocity. Otherwise, the tunnel ceiling is deflected to produce a weak pressure gradient. The aerodynamic conditions are as follows:

$$W_0 = 11.03\ \text{m/s}, \qquad U_e = 12.36\ \text{m/s}$$

$$\frac{\partial}{\partial x}\left(\frac{2p_e}{\rho U_e^2}\right) = -5.6 \times 10^{-3}\ \text{m}^{-1}, \qquad \pi = \frac{\delta_x}{\rho U_e^2}\frac{\partial P_e}{\partial x} \approx -0.01$$

$$\text{at } x = -2.5\ \text{mm}, \qquad \left(\frac{x}{\delta_0}\right) = -0.69$$

$$\delta_0 = 36\ \text{mm}\left(\frac{\bar{u}}{U_e} = 1\right), \qquad R_\theta = 3545$$

$$\text{at } x_f = 12\ \text{mm}, \qquad \left(\frac{x_f}{\delta_{0f}}\right) = 0.22$$

$$\delta_{0f} = 54\ \text{mm}, \qquad R_\theta = 5230$$

The measurements of the local flowfield along the explored zone, with and without rotation, have been carried out with a constant temperature anemometer. Measurements of longitudinal u' and transversal w' fluctuations have been performed by using a single straight hot wire rotating in a plane $(\boldsymbol{i}, \boldsymbol{k})$ parallel to the wall.[23] A data acquisition system enables a digital treatment taking into account, locally, the influence of the velocity component tangential to the wire. In the measurements the coefficient k (Ref. 24) can be defined from the effective cooling velocity

$$V_{\text{eff}} = \left[|V_N|^2 + k^2|V_T|^2\right]^{\frac{1}{2}} \tag{1}$$

where $V(t)$ is the instantaneous velocity. See the Appendix.

V_N and V_T are, respectively, the velocity components normal and tangential to the wire. The first set of measurements has been carried along the rotating cylinder in order to compare our results to those obtained in the IRPHE. In the general manner, the results are similar. In particularly, the reorganization of the flow into a two-dimensional boundary layer within a relative system tied to the rotating wall was obtained at $x/\delta_0 = 26.4$.

At the stationary part the flowfield was surveyed on seven axially sections and described with and without rotation of the upstream cylinder. Before getting into the detail of the obtained results, the analysis of the flow on the fixed part downstream the rotating cylinder has three zones: a zone close to the wall where the fluid responds to the new boundary conditions (cessation of spin), an adjacent zone of influence that remains affected by the rotation, and then comes the undisturbed external zone where the flow remains in equilibrium (Fig. 2).

III. Mean Flowfield

The analysis of the mean flowfield begins with the determination of the streamlines deviation angle β. To account for the degree of the three-dimensionality of the flow on the rotating cylinder, a relative coordinate system linked to the mobile wall is adopted in the rotation layer.[16]

As usual for three-dimensional flows, we have considered a polar representation in hodograph plane. Figure 3 shows the definitions of various angles and velocities. The mean velocity vector $\bar{\boldsymbol{q}}$ makes an angle β with the axial direction and γ, defined from the direction of the relative mean outer velocity $q_e(U_e, -W_0)$, is significant of the three-dimensionality of the mean velocity field.

On the fixed part downstream of the rotating cylinder, the streamline deviation persists in the neighboring regions; however, a relative

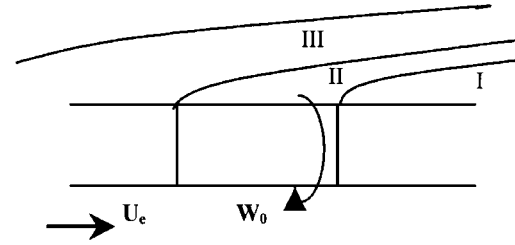

Fig. 2 Schematic structure of the boundary layer: I, influenced zone; II, rotating layer; and III, developed boundary layer.

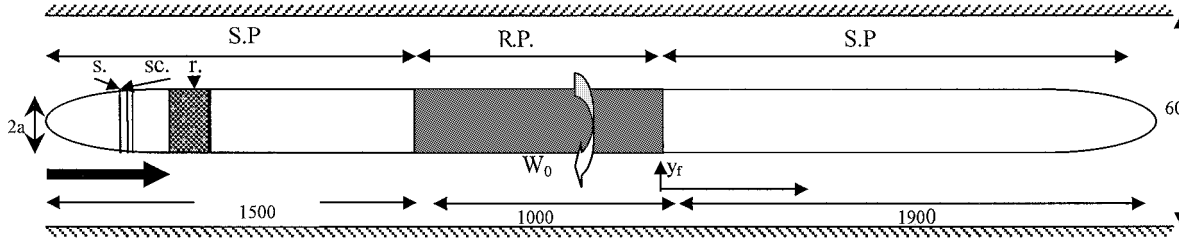

Fig. 1 Schematic arrangement of apparatus (dimensions in millimeters): r, roughness; s, stripe; sc, square grooves; S.P., stationary part; and R.P., rotating part.

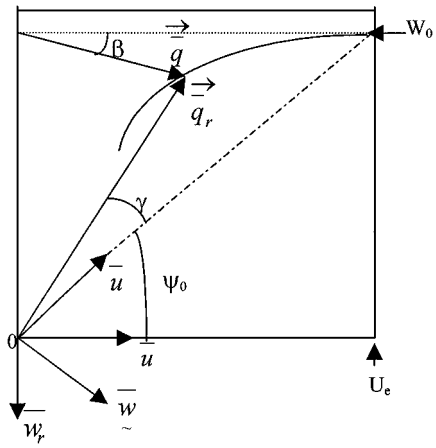

Fig. 3 Definitions of angles and velocities.

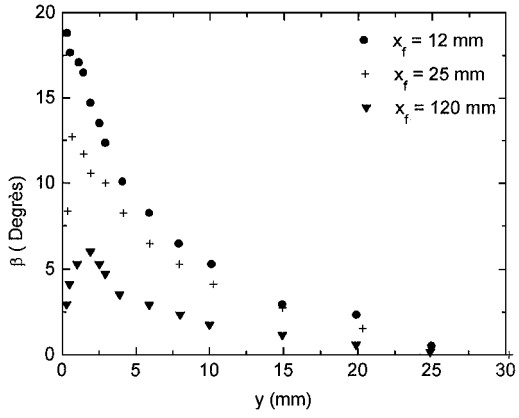

Fig. 4 Radial evolution of angle β on the downstream fixed part.

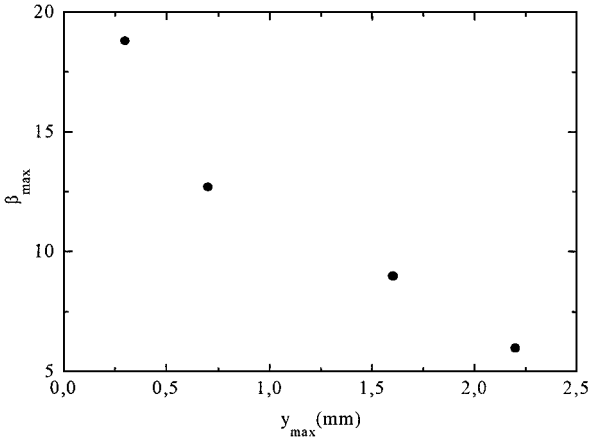

Fig. 5 β_{max} evolution as a function of y_{max} with longitudinal distance x_f.

coordinate system cannot be considered, and the γ and β angles are confused. Figure 4 represents the radial evolution of the angle β at different sections.

We observe globally that, because of the cessation of spinning, β is weak close to the wall, tends to reach a maximum β_{max} at y_{max}, and decreases to cancel at $y = 0,\ 6\delta$. We note furthermore that β_{max} decreases and y_{max} increases away from the rotating part of the cylinder (Fig. 5); therefore, the influence of the upstream rotation moves outward from the wall and then disappears at relatively distanced sections.

To analyze the degree of three-dimensionality of the flow on the rotating cylinder in a relative coordinate system and on the downstream fixed cylinder, we present in Fig. 6 the maximum deviation

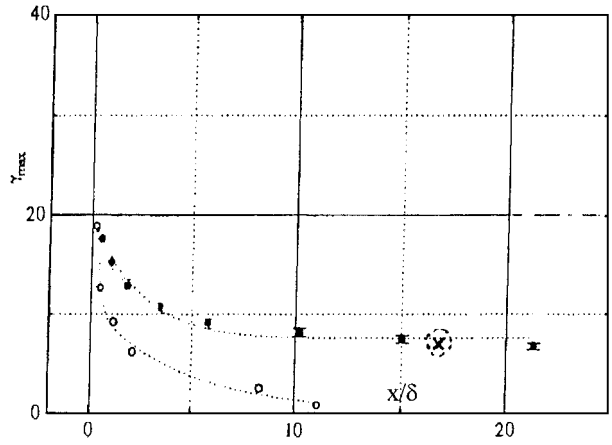

Fig. 6 Longitudinal evolution of γ_{max}.

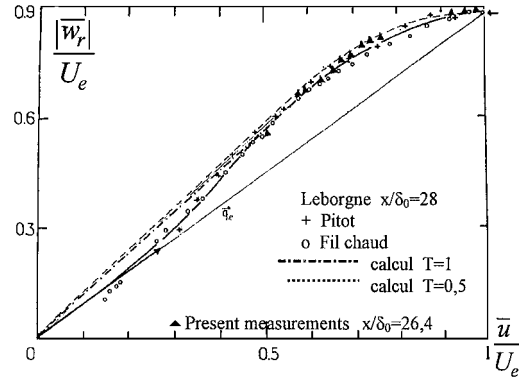

Fig. 7 Polar profile evolution on the rotating cylinder.

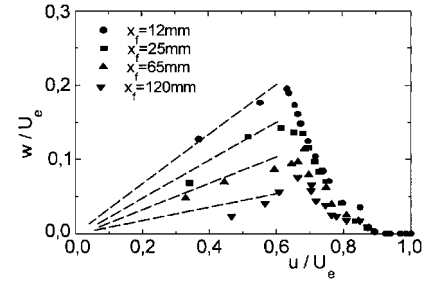

Fig. 8 Longitudinal evolution of the hodograph on the downstream fixed part.

γ_{max} vs the distance x counted from the beginning of the considered part of the cylinder.

We notice that γ_{max}, at the beginning of the fixed part, is as important as in the beginning of the rotating cylinder and tends rapidly to zero at $x = 12\delta$. The longitudinal evolution of γ_{max} on the rotating cylinder is asymptotic.

Also, the rapid diminution of γ close to the wall, on the rotating cylinder, induces an inflectional behavior of the experimental polar profile[14] (Fig. 7). However the calculated hodograh[16] does not show a such behavior; it remains practically linear up $u/U_e = 0.5$.

The evolution of the polar profiles drives then to a different interpretation of the restructuring process, near the wall, in the calculation and the experience. Indeed, it would seem according to the experience that the return to a collateral boundary layer is established first far more rapidly near the wall and spreads then gradually in the boundary layer.

On the other hand, the calculations do not indicate a preferred tendency; the polar profile tends to its linear form in its totality.

On the fixed part downstream of the rotating cylinder, the evolution of the polar profiles (Fig. 8) shows that the flow is collateral at the wall. The hodograph (u vs w plane; both normalized by the

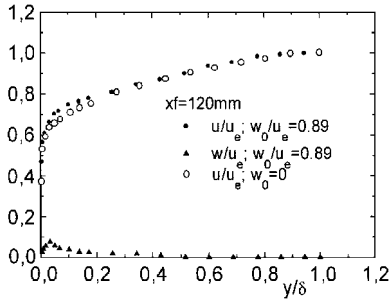

Fig. 9 Evolution of longitudinal and transversal velocity components on the downstream fixed part.

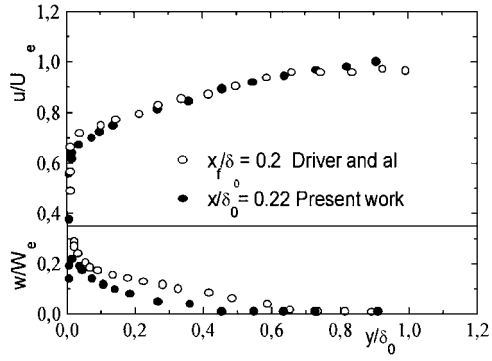

Fig. 10 Evolution of longitudinal and transversal velocity components on the downstream fixed part.

freestream velocity U_e) develops a classical triangular shape. The same feature is obtained from a bend configuration.[25] The apex of the triangle decreases with longitudinal distance. Near the wall, on the slow-speed side of the triangle ($u/U_e \leq 0.6$), the hodograph extrapolates to zero with the same slope as measured surface flow angle γ_{max}.

Measurements of angle β and mean velocity $\bar{q}$ of the distorted flow allows us to evaluate the longitudinal and transversal components of the velocity vector. Profiles of time averaged $\bar{u}$ and $\bar{w}$ velocities, in two cases of experience, are shown in Fig. 9. The streamwise component of the velocity u reveals a small acceleration in the internal zone of the boundary layer when the rotation is on.

The spanwise component of velocity reaches a maximum of approximately 25% of the freestream velocity component at the leading edge of the fixed part.

The peak in the crossflow defines the sign of the near-wall streamwise vorticity.[26] The near-wall streamwise vorticity is positive at wall normal distances below the peak in the crossflow profile and negative above the peak.

The results from Driver and Hebbar[21] are compared to ours. So, we note a good similarity in the velocity profiles presented in Fig. 10.

IV. Turbulent Flowfield

A. Second-Order Moments

Turbulent flowfield measurements, on the rotating cylinder, reveal an increase in $\overline{u'w'}$ covariance and in the variance $\overline{u'^2}$ and $\overline{w'^2}$. Nevertheless, at the farthest measure sections from the beginning of the rotation, the presentation of these results in the relative coordinate system shows that $\sqrt{(u'^2)}/q_e$ and $\sqrt{(w'^2)}/q_e$ are practically the same as those of the no-rotating case[21] (Fig. 11); $\overline{u'w'}$ profiles show the same trend (Fig. 12).

This shows that, in the relative coordinate system, the reorganization of the boundary layer in a two-dimensional flow is in a well-advanced phase. On the contrary, nearer the leading edge of the spinning, part the trend to the two-dimensionality of the turbulence intensities is in defect everywhere, except close to the wall in the inner part of the rotation layer.

On the stationary part, downstream of the spinning section, the results reveal a similar behavior of turbulence intensities and the $\overline{u'w'}$ covariance when the rotation is on. This effect is confined in

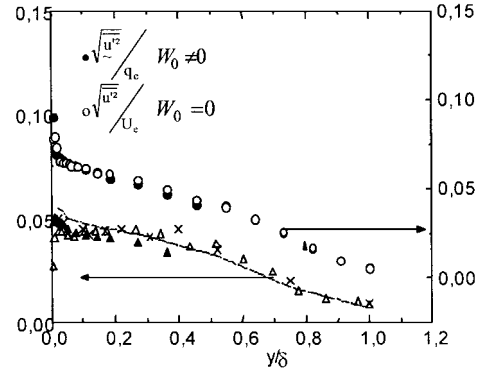

Fig. 11 Evolution of turbulence intensities on the rotating cylinder at $x/\delta_0 = 26.4$: △, $\sqrt{(w'^2)}/U_e$ $W_0 = 0$; ▲, $\sqrt{(w'^2)}/q_e$, present work $W_0 \neq 0$; ×, $\sqrt{(w'^2)}/U_e$ $W_0 = 0$; - - -, $\sqrt{(w'^2)}/q_e$, Arzoumanian $W_0 \neq 0$.

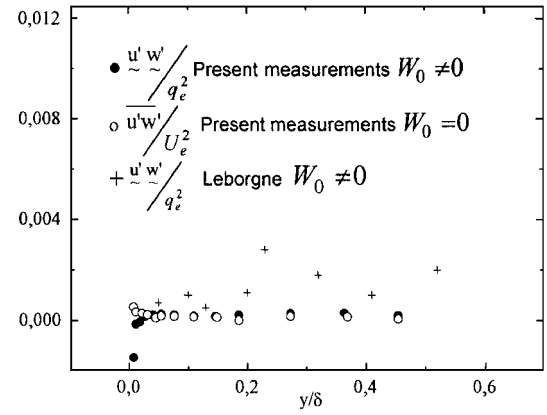

Fig. 12 Evolution of $u'w'$ correlation on the rotating cylinder at $x/\delta_0 = 26$.

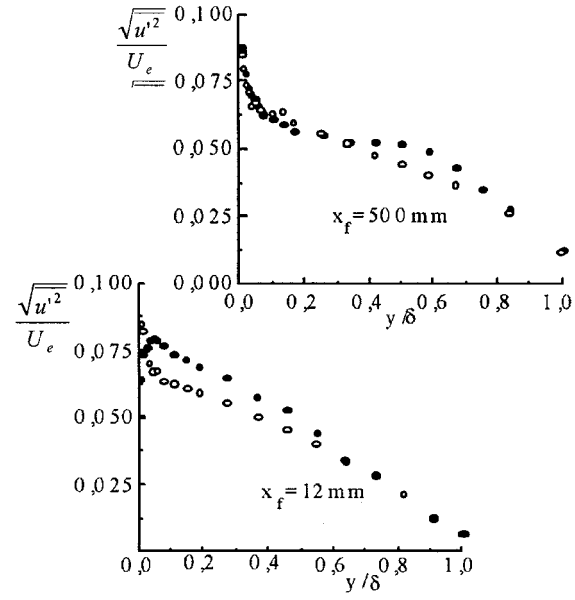

Fig. 13 Evolution of longitudinal turbulence intensity profiles on the fixed part.

a region qualified as "affected zone," which spreads at $y = 0.6\delta$ to 0.7δ. This zone, strongly affected by the rotation, would be the seat of a mechanism of supplementary turbulent production. This is provoked by the arrival of more energetic fluid masses from upstream region where the rotation is applied.

As the longitudinal distance x_f increases, the affected zone is found far from the cylinder surface. We believe that the fluid masses influenced by the upstream rotation move away from the wall during their longitudinal displacement. Furthermore Fig. 13 shows a

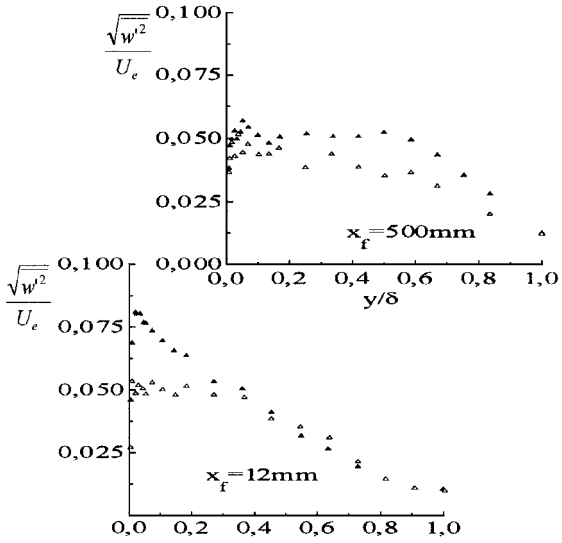

Fig. 14 Evolution of transversal turbulence intensity profiles on the downstream fixed part.

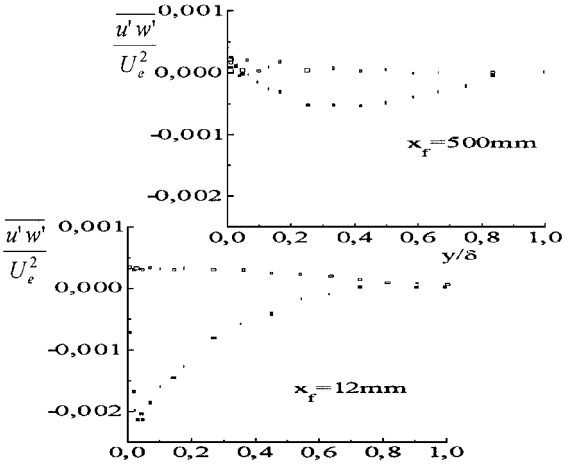

Fig. 15 Evolution of $\overline{u'w'}$ correlation profiles on the downstream fixed part.

maximum of turbulent intensity at y_{ext} position, different from that obtained for the rotationless case that occurs nearer the wall. This effect decreases in intensity and disappears for large distances x_f. The same trend is observed by Flack and Johnston[25] in v'^2 profiles. The location of the v'^2 maximum shifts farther out in the boundary layer. We think that during their projection the local structures interact with structures influenced by the rotation and constitute zones of active motions with strong intensity in the vicinity of y_{ext}.

Figure 14 points out the behavior of the transversal turbulence intensity in the same positions. Contrary to what is observed on the longitudinal turbulence intensity, the influence persists in the vicinity of the wall when we get away from the spinning part. Such behavior would indicate that the evolution of the previous structures, according to the two considered directions, is different. It seems that as structures move away from the wall they twist and contaminate the under regions in the transverse direction.

The Schwarz and Bradshaw[27] near-wall investigation in a bend configuration showed an increase in u'^2 and w'^2, which is attributed to increased production. The turbulent kinetic energy (TKE) profiles predicted by Olçmen and Simpson[28] show that, at successive locations in sheared boundary layer, the TKE of the flow increases near the wall but decreases away from the wall. Figure 15 points out the evolution of the correlation $\overline{u'w'}$ profiles in two experimental cases.

In the rotationless case the weak level of values observed confirms the two-dimensionality of the flow. When spinning is applied, we note a net increase of the $\overline{u'w'}$ correlation in the "influenced zone"; the flow structure is very affected by the upstream rotation. Some

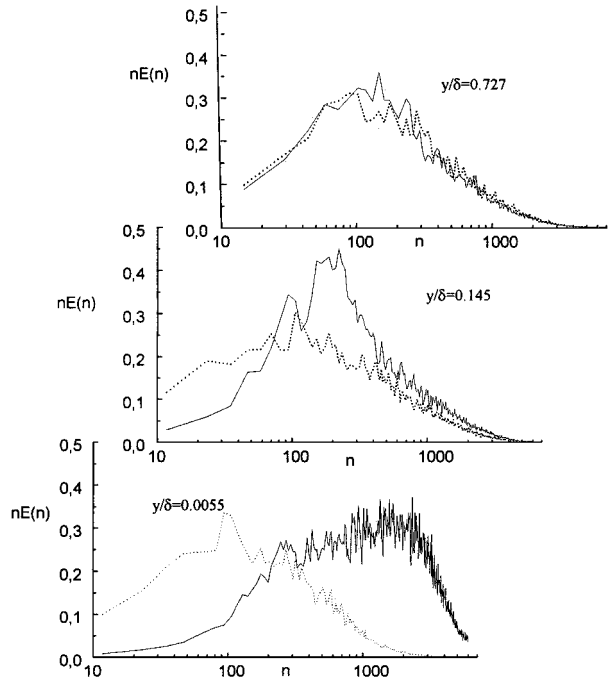

Fig. 16 Radial evolution of energy spectrum on the rotating cylinder at $x/\delta_0 = 26.4$.

complex three-dimensional effects are introduced; however, these attenuate at the farthest sections.

Flack and Johnston[25] noticed that $\overline{u'w'}$ decreased in the near-wall region with increased three-dimensionality, and the trend reversed in the outer part of the boundary layer. So, to better analyze the spinning effects on self time correlation, a spectral study is undertaken.

B. Spectral Analysis

On the spinning cylinder one observes (Fig. 16) that the rotation introduces a shift of energy spectrum of q vector fluctuations to high frequencies much more than one decade. Lohmann[10] has obtained a similar result. He attributed to a degradation of turbulent structures in smaller scales. Nevertheless, according to the analysis undertaken at the IRPHE this strong translation was rather attributed to the passage, ahead of the detector, of parietal structures. Indeed, the maximal frequency value of energy spectrum (spectral peaks) varies with wall speed W_0.[17,18]

When we get away from the wall, the structures lose their coherence, and the detector perceives less frequently their passage; this implies an evolution of spectra to low frequencies, and thus spectra measured in the rotation case tend to join the no-rotation case outside the rotation layer.

The longitudinal and transverse fluctuation spectrum evolutions are examined in the relative coordinate system. We have determined by numerical filtering on energy spectrum Eq.'(n) weighted by the variance, each frequency component contribution to the longitudinal an transversal turbulence intensities. The spectra in the rotating system show that the frequency discrepancy persists (Fig. 17). On the fixed part, at $x_f = 12$ mm, energy spectrum remains affected by upstream spinning in the internal region (affected zone) (Fig. 18). At a farthest station $x_f = 120$ mm, we observe that in the vicinity of the wall spectra obtained in the two experimental cases are almost similar (Fig. 19).

The zone close to the wall seems a little sensitive to the spinning effect, therefore, as the preceding results concerning turbulence intensities show. The size of this unaffected region is larger as the longitudinal distance x_f increases.

Indeed at $x_f = 700$ mm the rotation effect occurs only for a distance far enough from the wall such as $y = 0.3\delta$, and it remains nevertheless minimal (Fig. 20). Structures already specified, responsible of the contribution in energy over spectra, tend to leave the wall during their longitudinal displacement. This translation would be traduced then into a diffusion of kinetic turbulence energy far from

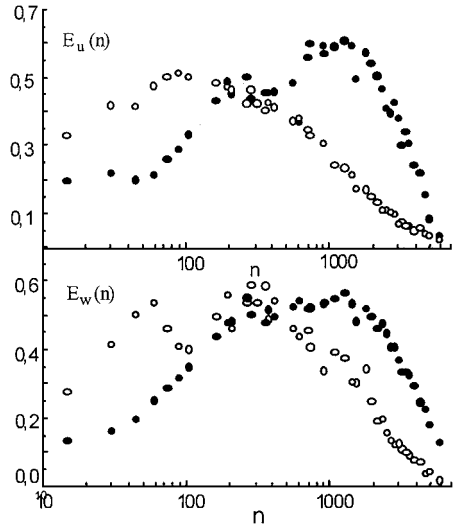

Fig. 17 Energy spectrum of u' and w' components on the rotating cylinder (in relative coordinate system).

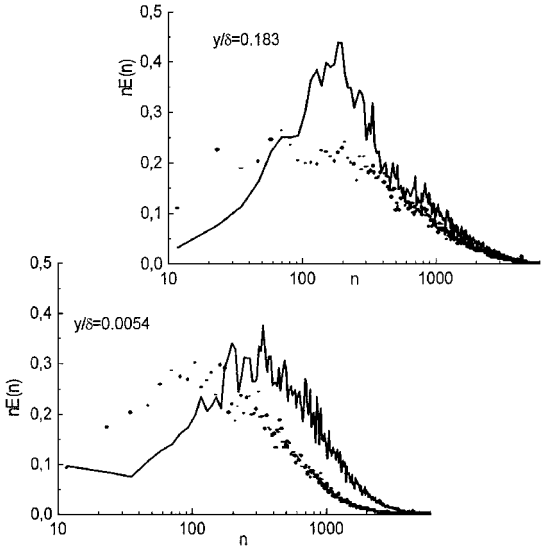

Fig. 18 Radial evolution of energy spectrum on the downstream fixed part at $x_f = 12$ mm.

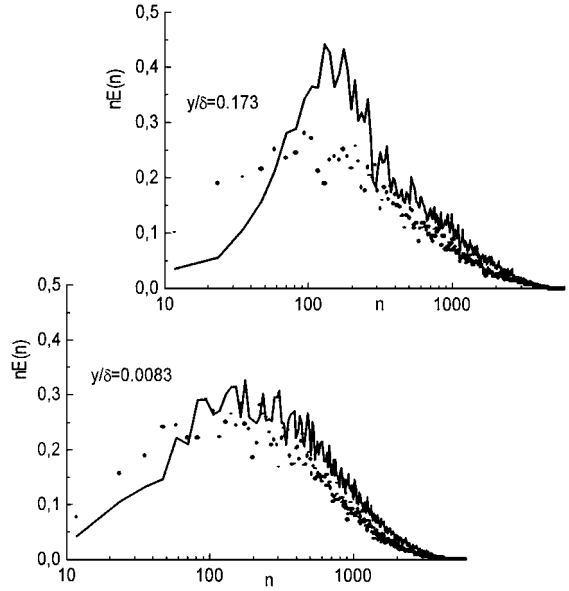

Fig. 19 Radial evolution of energy spectrum on the dowstream fixed part at $x_f = 120$ mm.

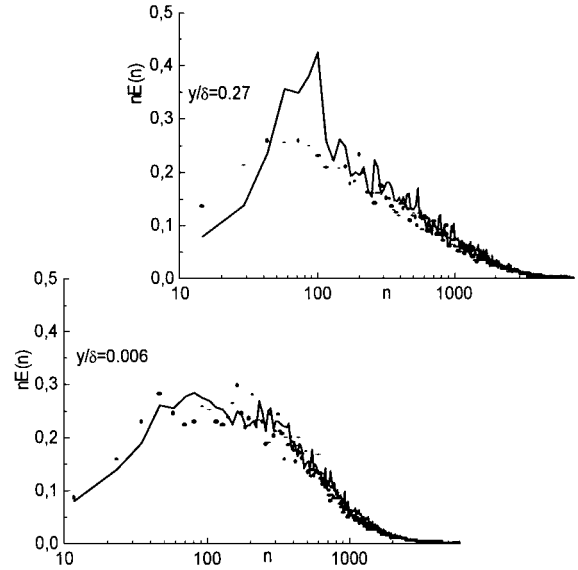

Fig. 20 Radial evolution of energy spectrum on the downstream fixed part at $x_f = 700$ mm.

the wall. This hypothesis agrees well with the $v'k/U_e^2 = f(y/\delta)$ profiles given by Driver and Hebbar.[21]

C. Turbulence Length Scales

To complete the analysis of the flow and to understand the phenomena of such complex behavior, we have evaluated the turbulence scales on the spinning part as well as on its endorsement. To determine space integral scales characterizing big eddies, we considered Taylor's hypothesis of coagulated turbulence field. With this hypothesis we consider an equivalence between a temporal recording and an instantaneous spatial recording; $\Lambda = T \cdot u_c$, where u_c is the structure convection velocity, which remains more or less equal to the local mean velocity of flow,[29] and

$$T = \int_0^\infty \frac{\overline{s'(t)s'(t+\tau)}}{\overline{s'^2}}\,\mathrm{d}\tau$$

Furthermore, the Taylor microscale λ is given by $\lambda = \bar{u}/2\pi N$; N is the equivalent frequency defined by

$$N^2 = \int_0^\infty n^2 E(n)\,\mathrm{d}n$$

the spectral function $E(n)$ is such that

$$\int_{-\infty}^{+\infty} E(n)\,\mathrm{d}n = 1$$

The radial evolution of integral scale Λ, in two different experiences ($W_0 = 0$ and $W_0 \neq 0$), is shown in Fig. 21 on the downstream fixed part. Without rotation the evolution of the integral scale relative to longitudinal fluctuation u' is similar to that obtained for the flat-plane boundary layer.[30]

When rotation is applied, Λ_q relative to q' fluctuation decreases on the two explored parts of the cylinder. This effect remains nevertheless more pronounced in the rotation layer: on the spinning cylinder (Fig. 22). In fact, the observed effect is associated with the diminution of the correlation time T (Fig. 23). The evolution of the microscale λ in the influenced zone and in the rotation layer shows that λ decreases when rotation is on (Fig. 24), but in lesser proportions as compared to the integral scale Λ.

The results obtained by Piomelli et al.[31] indicate that the small scales tend to adapt to the perturbation much faster than the large scales. The large decrease of λ means that the dissipation rate $\varepsilon/\overline{u^2}$ is increased. The contribution in energy observed on spectra, in the equilibrium frequency range, would be accompanied by an increase of ε. The Smagorinsky model applied by Piomelli et al.[31]

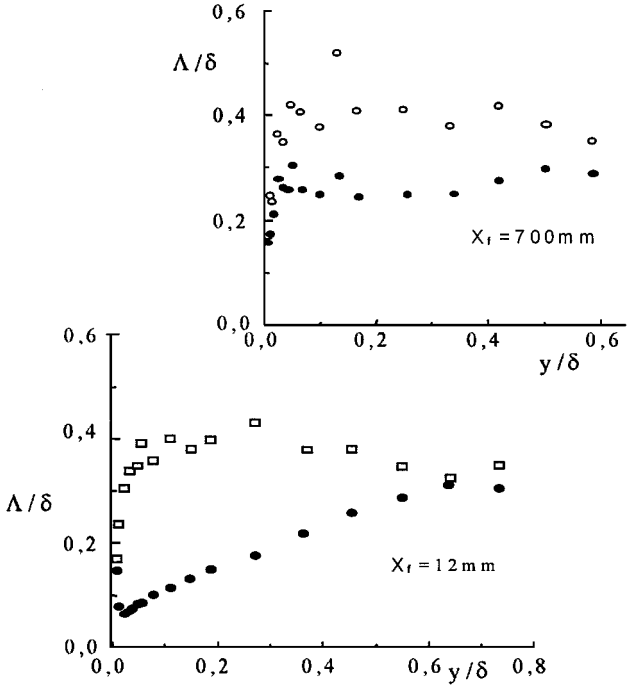

Fig. 21 Integral scale evolution on the fixed part.

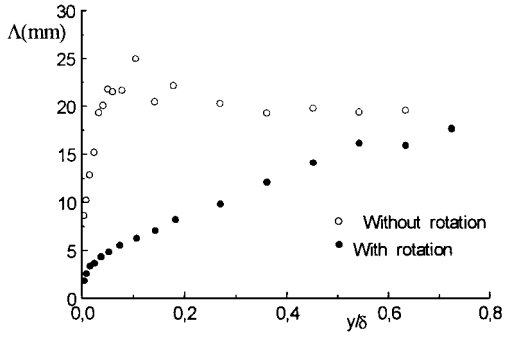

Fig. 22 Integral scale at $x/\delta_0 = 26.4$ on the rotating cylinder.

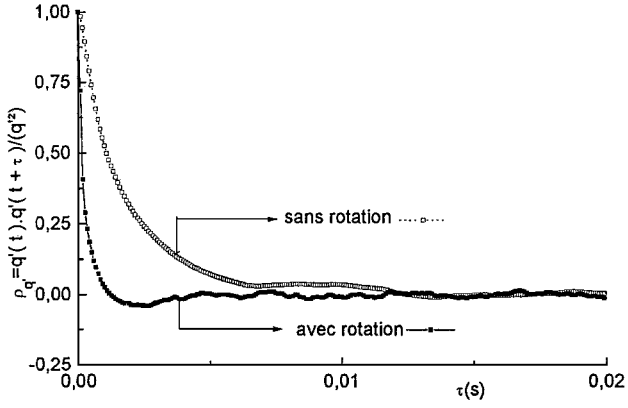

Fig. 23 Coefficient of the correlation on the rotating cylinder at $x/\delta_0 = 26, 4$.

predicts an increased production in the near-wall region, reflecting the imposition of the transverse shear $\partial\bar{w}/\partial y$.

In zones characterized by an increase in turbulence intensities—rotation on, we examine the variation of $R\lambda/\Lambda$, which is often used to characterize the turbulent field. This product is generally invariant in the external zone of the boundary layer and equals $15/A$ ($A \approx 1$).[32] Without rotation one observes that the evolution of $R\lambda/\Lambda$ is similar to that obtained in a pipe flow[33] (Fig. 25). In the external zone of the boundary layer, $R\lambda/\Lambda$ evolves around an average value of 20. When rotation is on, $R\lambda/\Lambda$ increases despite the diminution observed in R. Then, the effect of rotation is explained by the increase of the turbulence intensity q'^2, which is more important then the diminution of λ and Λ.

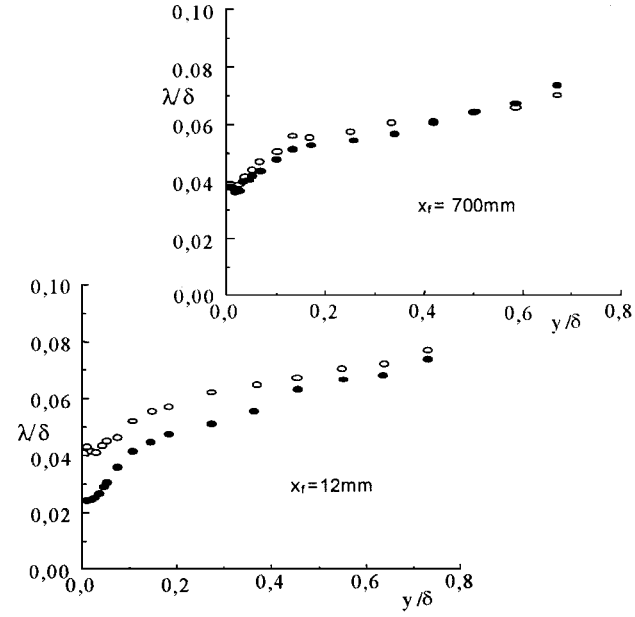

Fig. 24 Microscale evolution on the fixed part.

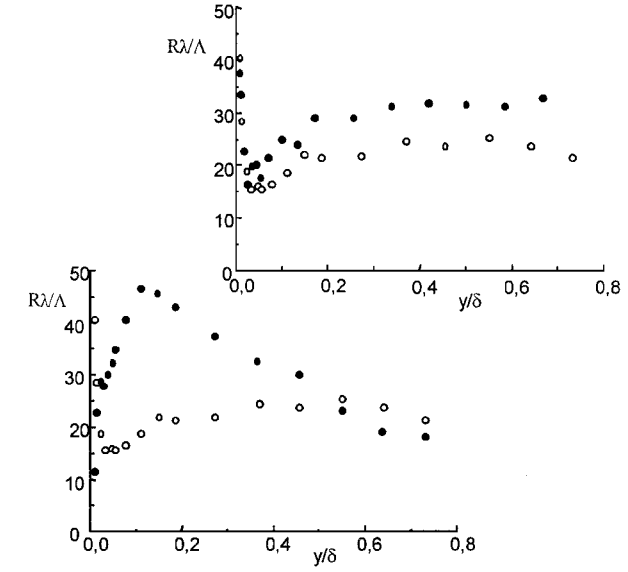

Fig. 25 $R\lambda/\Lambda$ evolution on the fixed part: ●, $W_0 \neq 0$ and ○, $W_0 = 0$.

It is admitted[31] that the turbulence production, in shear flows, increases the level of turbulence. Indeed, the diminution of the correlation is much strong more the velocity gradient is highest; we suppose then that the diminution of turbulence scales is directly linked to the supplementary transverse distortion $\partial\bar{w}/\partial y$.

V. Conclusions

The relaxation of a three-dimensional, shear-driven turbulent boundary layer to a two-dimensional layer was experimentally studied to better understand the turbulent transport processes. Flow initially swirling about a spinning cylinder passes over a stationary section. This passage produces a sudden change in boundary condition. Three zones appear: an interaction zone where the flow responds to the new boundary conditions (cessation of spin), an adjacent one where the influence of the rotation remains persistent on the flow structure, and an outer undisturbed zone where the flow remains in equilibrium. The recovery to a two-dimensional boundary layer starts in the near-wall region and diffuses outward from the wall.

The process of energy production induced by the rotation in the influenced zone, and which is important on the rotating part, spreads to a relatively downstream sections. This is caused by the passage of more energetic fluid masses from the upstream region. The spectrum shift exists even if we consider the relative coordinate system on the spinning part. The result calls into question whether spectrum shift is solely caused by the passage of structures ahead of the detector. The remarkable diminution of the integral length scale suggests that the rotation favors the evolution of large structures toward finer ones. This confirms the interpretation advanced previously by Lohmann.[10]

Appendix: Calculation Method

We recall briefly in this section the calculation method to get the different components of the velocity field. The King law is $E^2 = A_c + B_c V_{\text{eff}}^n$; A_c, B_c, and n are the calibration constants. We consider the case that $\bar{q}$ deviates of an angle β relatively to the longitudinal direction $\boldsymbol{i}$. $(\boldsymbol{I}, \boldsymbol{J}, \boldsymbol{K})$ system is deduced by a rotation of an angle β for $(\boldsymbol{i}, \boldsymbol{j}, \boldsymbol{k})$ system, $\vec{\text{proj}} V(t)(\bar{q} + q', w'_f)$ on the $(\boldsymbol{I}, \boldsymbol{K})$ plane. We deduce then

$$q' = u' \cos\beta + w' \sin\beta \qquad w'_f = -u' \sin\beta + w' \cos\beta$$

$V(t)(\bar{q} + q', v', w'_f)$, $f(\sin\varphi, 0, \cos\varphi)$. According to Eq. (1),

$$V_{\text{eff}}^2 = v'^2 + [w'_f \sin\varphi - (\bar{q} + q')\cos\varphi]^2 + k^2[(\bar{q} + q')\sin\varphi + (w'_f \cos\varphi)]^2$$

After developing the calculation and neglecting the terms of order two, we obtain

$$V_{\text{eff}} = \bar{q}\cos\varphi(1 + k^2 tg^2\varphi)^{\frac{1}{2}}\left[1 + \frac{q'}{\bar{q}} - \frac{w'_f}{\bar{q}} tg\varphi\left(\frac{1 - k^2}{1 + k^2 tg^2\varphi}\right)\right]$$

We pose

$$a = \frac{1 - k^2}{1 + k^2 tg^2\varphi}, \qquad b = (1 + k^2 tg^2\varphi)^{\frac{1}{2}}$$

We obtain

$$V_{\text{eff}} = \bar{q} b \cos\varphi\left[1 + q'^2/\bar{q} - (w'_f/\bar{q}) a tg\varphi\right] = C \tag{A1}$$

On the other hand,

$$V_{\text{eff}_i} = \left\{\left[\left(E_i^2 - A\right)/B\right]\right\}^{1/n}$$

At the position $\varphi = 0$,

$$\bar{q} = \frac{1}{N}\sum_{i=1}^{N}\left(\frac{E_i^2 - A}{B}\right)^{1/n}$$

N is the total number of the acquisition points. At the position $\varphi \neq 0$,

$$\frac{1}{N}\sum_{i=1}^{N}\left(\frac{E_i^2 - A}{B}\right)^{1/n} = C = \bar{q}\cos\varphi(1 + k_2 tg_2\varphi)^{\frac{1}{2}}$$

$$\Rightarrow k^2 = \frac{1}{tg^2\varphi}\left\{\left[\frac{1}{\bar{q}\cos\varphi}\frac{1}{N}\sum_{i=1}^{N}\left(\frac{E_i^2 - A}{B}\right)^{1/n}\right]^2 - 1\right\} \tag{A2}$$

According to Eq. (A2),

$$\overline{V_{\text{eff}}} = \bar{q} b \cos\varphi \cdot v'_{\text{eff}} = V_{\text{eff}} - \bar{V}_{\text{eff}} = Au' + Bw'$$

with

$$A = b[\cos(\beta - \varphi) + (a - 1)\sin\beta\sin\varphi]$$

$$B = b[\sin(\beta - \varphi) - (a - 1)\cos\beta\sin\varphi]$$

It implies then that

$$\overline{v'^2_{\text{eff}}} = A^2\overline{u'^2} + B^2\overline{w'^2} + 2AB\overline{u'w'}$$

The velocity vector components $\underline{\bar{u}}$ and $\underline{\bar{w}}$ in the rotating system with the cylinder $\underline{S}$ are deduced from $(\bar{u}, \bar{w} - w_0)$ by a rotation of angle Ψ_0:

$$\cos\Psi_0 = U_e/Q_e, \qquad \sin\Psi_0 = -W_0/Q_e$$

We obtain then

$$\underline{\bar{u}} = (U_e/Q_e)\bar{u} - (W_0/Q_e)(\bar{w} - W_0)$$

$$\underline{u} = (U_e/Q_e)u' - (W_0/Q_e)w', \qquad \underline{\bar{v}} = \bar{v}, \qquad \underline{v}' = v'$$

$$\underline{\bar{w}} = (W_0/Q_e)\bar{u} + (U_e/Q_e)(\bar{w} - W_0)$$

$$\underline{w}' = (W_0/Q_e)u' + (U_e/Q_e)w'$$

Acknowledgment

In the context of Project 01 MDU526, financial support for the paper was provided by the Commission Mixte d'Evaluation de Projets and is gratefully acknowledged.

References

[1] Launder, B. E., "Turbulence Modeling of Three-Dimensional Shear Flows," CP-438, AGARD, 1988.

[2] Purtell, L. P., "Turbulence in Complex Flows: A Selected Review," AIAA Paper 92-0435, 1992.

[3] Elsenaar, A., and Boelsma, S. H., "Measurements of Reynolds Stress Tensor in a Three Dimensional Turbulent Boundary Layer Under Infinite Swept Wing Conditions," National Aerospace Lab., NLR TR 74095 U, The Netherlands, 1974.

[4] Muller, U., "Measurements of the Reynolds Stresses and the Mean Flow Field in a Three Dimensional Pressure Driven Boundary Layer," *Journal of Fluid Mechanics*, Vol. 119, 1982, pp. 121–153.

[5] Bradshaw, P., and Pontikos, N. S., "Measurements in Turbulent Boundary Layer on an Infinite Swept Wing," *Journal of Fluid Mechanics*, Vol. 159, 1985, pp. 105–130.

[6] Bradshaw, P., and Terrell, M. G., "The Response of a Turbulent Boundary Layer on an Infinite Swept Wing to a Sudden Removal of Pressure Gradient," NPL Aero. Rept. 1305, 1969.

[7] Olçmen, S. M., and Simpson, R. L., "An Experimental Study of a Three-Dimensional Pressure Driven Turbulent Boundary layer," *Journal of Fluid Mechanics*, Vol. 290, 1995, pp. 225–262.

[8] Furuya, Y., and Nakamura, I., "Velocity Profiles in the Skewed Boundary Layers on Some Rotating Bodies in Axial Flow," *Journal of Applied Mechanics*, March 1970, pp. 17–24.

[9] Bissonette, L., and Mellor, G. L., "Experiments on the Behavior of an Axisymmetric Turbulent Boundary Layer with a Sudden Cirumferential Strain," *Journal of Fluid Mechanics*, Vol. 63, Pt. 2, 1974, pp. 369–413.

[10] Lohmann, R. P., "The Response of a Developed Turbulent Boundary Layer to Local Transverse Surface Motion," *Journal of Fluid Engineering*, Vol. 98, 1976, pp. 354–363.

[11] Arslanian, G., "Champ de Vitesse Moyenne d'une Couche Limite sur un Cylindre en Rotation dans un Écoulement Axial," Ph.D. Dissertation, 3rd Cycle, Inst. de Mécanique Statistique de Turbulence, Université d'Aix Marseille II, Marseille, France, Sept. 1976.

[12] Arzoumanian, E., Fulachier, L., and Dumas, R., "Experimental Investigation of the 3DTBL of an Axially Rotated Cylinder," *Proceeding of 2nd International Symposium on Turbulent Shear Flows*, London, 1979, pp. 4.28–4.33.

[13] Arzoumanian, E., Fulachier, L., and Cousteix et Aupoix, B., "Couche Limite Turbulente Tridimensionnelle: Restructuration d'un Écoulement Axisymetrique Soumis à une Discontinuité de la Vitesse à la Paroi," CP 217, AGARD, 1979, pp. 19.1–19.11.

[14] Leborgne, L., "Contribution à l'Étude d'une Couche Limite Turbulente Soumise à une Brusque Continuité à la Paroi," Ph.D. Dissertation, 3rd Cycle, Inst. de Mécanique Statistique de Turbulence, Université d'Aix Marseille II, Marseille, France, Sept. 1981.

[15] Arzoumanian, E., Leborgne, M., and Fulachier, L., "Turbulent Field of a Boundary Layer very Close to an Axially Rotated Cylinder," 3rd Symposium on Turbulent Shear Flows, Sept. 1981.

[16] Arzoumanian, E., Fulachier, L., and Dumas, R., "Couche Limite Turbulente sur Paroi Mobile: Effet Spectral," *Comptes Rendus de l'Académie des Sciences*, Serie 2, Sept. 1983, pp. 203–208.

[17]Collini, P., Fulachier, L., and Dumas, R., "Visualization of Streaky Pattern Within a Turbulent Boundary Layer on a Moving Wall," *Euromech Colloquium 202*, NLR, North East Polden, The Netherlands, 1985.

[18]Collini, P., and Fulachier, L., "Structure Striée d'une Couche Limite Turbulente sur Paroi Mobile Transversalement," *Comptes Rendus de l'Académie des Sciences*, Serie 2, No. 2, 1986, t302.

[19]Cousteix, J., Aupoix, B., Arzoumanian, E., and Fulachier, L., "Experimental and Numerical Investigation of a Turbulent Boundary Layer Subjected to a Sudden Transverse Strain," *Physics of Fluids*, Vol. 26, No. 9, 1983, pp. 2399–2407.

[20]Dumas, R., Arzoumanian, E., and Fulachier, L., "Couche Limite sur Paroi Mobile," *Journal de Mécanique Théorique et Appliquée*, Vol. 7, No. 5, 1988, pp. 507–530.

[21]Driver, D. M., and Hebbar, S. K., "Experimental Study of Three-Dimensional Shear Driven, Turbulent Boundary Layer," *AIAA Journal*, Vol. 25, No. 1, 1987, pp. 35–42.

[22]Higuchi, H., and Rubesin, M. W., "Behavior of a Turbulent Boundary Layer Subjected to Sudden Transverse Strain," *AIAA Journal*, Vol. 17, No. 9, 1979, p. 931.

[23]Fujita, H., and Kovasznay, L.S.G., *Rev. Sci. Inst.* Vol. 39, 1968.

[24]Champagne, F. H., "Turbulence Measurements with Inclined Hot Wire," Boeing Science Res. Lab., Rept. 103, 1965.

[25]Flack, K. A., and Johnston, J. P., "Near-Wall Flow in Three-Dimensional Boundary Layer on the End Wall of a 30° Bend," *Experiments in Fluids*, Vol. 24, 1998, pp. 175–184.

[26]Flack, K. A., "Near-Wall Structure of Three-Dimensional Turbulent Boundary Layers," *Experiments in Fluids*, Vol. 23, 1997, pp. 335–340.

[27]Schwarz, W. R., and Bradshaw, P., "Turbulence Structural Changes for a Three-Dimensional Turbulent Boundary Layer in a 30° Bend," *Journal of Fluid Mechanics*, Vol. 272, 1994, pp. 183–209.

[28]Olçmen, S. M., and Simpson R. L., "An Experimental Study of a Three-Dimensional Pressure Driven Turbulent Boundary Layer," *Journal of Fluid Mechanics*, Vol. 290, 1995, pp. 225–262.

[29]Cousteix, J., *Turbulence et Couche Limite*, Cepadues-Editions, Paris, 1989.

[30]Fulachier, L., "Contribution à l'Étude des Analogies des Champs Dynamique et Thermique dans une Couche Limite Turbulente: Effet de l'Aspiration," Thèse de Doctorat d'état es-Sciences Physiques, Université de Provence, Marseille, France, 1972.

[31]Piomelli, U., Colema, G. N., and Kim, J., "On the Effects of Nonequilibrium on the Subgrid-Scale Stresses," *Physics of Fluids*, Vol. 9, 1997, pp. 2740–2748.

[32]Favre, A., Kovasznay, L. S. G., Dumas, R., Gaviglio, J., and Coantic, M., *La Turbulence en Mécanique des Fluides*, Bordas, Paris, 1976, Chap. 3.

[33]Elena, M., "Etude des Champs Dynamique et Thermique d'un Écoulement Turbulent en Conduite avec Aspiration à la Paroi," Thèse de Doctorat es Sciences Physiques, Univ. de Provence, Marseille, France, July 1975.

P. R. Bandyopadhyay
Associate Editor